Natural Hazards
and Earth System
Sciences

Open Access

Discussions

The simultaneous occurrence of surge and discharge extremes for the Rhine delta

S. F. Kew, F. M. Selten, G. Lenderink, and W. Hazeleger

Royal Netherlands Meteorological Institute, De Bilt, The Netherlands

Correspondence to: S. F. Kew (sarah.kew@wur.nl)

Discussion Paper | Discussion Paper | Discussion Paper | Discussion Paper |

NHESSD

1, 111–141, 2013

Simultaneous occurrence of surge and discharge extremes

S. F. Kew et al.

Title Page

Abstract | Introduction

Conclusions | References

Tables | Figures

◄ | ►

◄ | ►

Back | Close

Full Screen / Esc

Printer-friendly Version

Interactive Discussion

Abstract

The low-lying Netherlands is at risk from multiple threats of sea level rise, storm surges and extreme river discharges. Should these threats occur simultaneously, a catastrophe will be at hand. Knowledge about the likelihood of simultaneous occurance or the so-called "compound effect" of such threats is essential to provide guidance on legislation for dike heights, flood barrier design and water management in general.

In this study, we explore the simultaneous threats of North Sea storm surges and extreme Rhine river discharge for the current and future climate in a large 17-member global climate model ensemble. We use a simple approach, taking proxies of North-Northwesterly winds over the North Sea and multiple-day precipitation averaged over the Rhine basin for storm surge and discharge respectively, so that a sensitivity analysis is straight forward to apply. By investigating soft extremes, we circumvent the need to extrapolate the data and thereby permit the synoptic development of selected events to be inspected.

Our principle finding is that, for the current climate, the probability of extreme surge conditions following extreme 20-day precipitation sums is around 3 times higher than that estimated from treating extreme surge and discharge probabilities as independent, as previously assumed. For the future climate, the assumption of independence cannot be rejected, at least not for precipitation sums exceeding 7 days.

1 Introduction

1.1 Storm surge barrier closure

The low-lying Netherlands is at risk from multiple threats of sea level rise, storm surges and extreme river discharges. The Maeslant storm surge barrier near Hoek van Holland, built to protect the densely populated Rotterdam area, closes automatically when the water level is predicted to exceed the current mean sea level by more than 3 m (Van

den Brink et al., 2005) – the 1/10 yr return level. The water level depends on both sea conditions (tide and surge) and the Rhine river discharge. The decision of if and when to close the barrier might be complicated in the case of a simultaneous extreme surge and extreme discharge event. In the event of an extreme discharge alone, the barrier

5 should remain open to prevent the damming of excess water. In the event of a joint event, the closed barrier would be at risk of failure due to a reversal of the pressure gradient at the barrier's base.

1.2 Surge-favourable meteorological situation

The Dutch coast is at risk from storm surges when strong North or Northwesterly winds

10 are present over the North Sea, as these wind directions have the largest fetch. The meteorological situation leading to these conditions and present in the highest observed (Van den Brink et al., 2004) and modelled (Van den Brink et al., 2004; Sterl et al., 2009) surges is a large-scale depression centred over or near southern Scandinavia. The largest modelled surge was accompanied by 3 hourly winds in excess of

15 45 kn (23 m s^{-1}) over the North Sea (Sterl et al., 2009).

1.3 The independence assumption and reported related research

Often the probabilities of the storm surges and high Rhine discharge are treated independently, assuming that the correlation between them is small, but the issue of independence is still under debate. It received renewed attention after a recent simul-

20 taneous surge and extreme discharge event on 5–6 January 2012. Leading up to this event, a westerly flow regime with an anomalously high NAO index (the 3-month running mean reached the highest since spring 1992), had brought a succession of precipitating systems over the Netherlands. In December 2011, twice the normal monthly precipitation sum was recorded in the North of the Netherlands, and during the first

25 week of January, 50–90 mm fell in 5 days – an event with a 1 in 5 to 1 in 20-yr return period (R. Sluijter, personal communication, 2012). The final storm with Northwesterlies

in its wake generated a high North Sea surge. Maeslant barrier closure came into discussion (but was not realised) and the surge prevented sluices in Friesland and Groningen from discharging to the sea for 5 consecutive tidal cycles and 8 in total (K.-J. Van Heeringen, Deltares, personal communication, 2012), creating havoc for the waterboards. The uneasiness generated by the assumption of independence stems not only from the risks implied if it is incorrect, but perhaps also a sense that it is counter-intuitive, as both surges and extreme discharge are frequently associated with present or recently present synoptic low pressure systems. We seek to investigate the independence assumption and present the results in a way that can be related to the intuitive expectation.

The recent study by Van den Brink et al. (2005), featuring a short assessment on storm surge barrier closure, finds no apparent positive correlation between the amplitude of North Sea surges and Rhine discharges. Most barrier-closure conditions in their data were caused by a high surge level and were relatively insensitive to extreme river discharge. They concentrated on 20-day precipitation sums accumulated over the Rhine basin and modelled the discharge at Lobith (a station upstream of the Rhine delta, near the Dutch-German border, Fig. 1) using an empirically tuned simple water balance equation, accounting for large-scale and convective precipitation, evaporation and snow accumulation (Van den Brink et al., 2005, Eq. 4). The high tide surge was calculated following Eq. (1) of Van den Brink et al. (2004) using the 12-h averaged wind speed and direction at a central grid box over the North Sea and the sea level pressure (SLP) (for the barometric pressure effect) at Hoek van Holland.

Van den Brink et al. (2005) took advantage of the large archive of ECMWF seasonal forecast ensemble runs (1987–2004) to obtain 1570 yr of data, which they regarded as independent due to the ensemble's low seasonal forecasting skill for the Netherlands. In this aspect, their study was a substantial step forward over previous work on joint probabilities (e.g. Van der Made, 1969) which had been limited by the very short observational times series of around 50 yr (although reaching the same conclusion). However, despite the adequately verified independence of the ensemble runs, they

admit that the initialisation period 1987–2004 might not be entirely representative of the full range of the present climate's variability.

Their conclusion that there is no positive correlation between the amplitude of North Sea surges and Rhine discharges is drawn from their Fig. 6b (Van den Brink et al., 2005), which displays a scatter plot of the water level at Hoek van Holland versus the Rhine discharge at Lobith. We note from the same figure, however, that the spread of sea levels does show some dependency on discharge. For example, the lowest sea levels are obtained only when the discharge is also low, and high discharges (limited data) occur only with medium-range sea-levels. The relationship between the extreme discharges and surges could be investigated more thoroughly. An examination of the synoptic situation for the extreme events would also give insight beyond correlation statistics into the physical evolution of the scenario and thus if and how a joint extreme event (simultaneous high discharge and storm surge) might occur.

1.4 Effect of a warming climate

Sterl et al. (2009) conducted a study of extreme North Sea surges by forcing a surge model with meteorological input from ESSENCE, a 17-member ensemble of the ECHAM5/MPI global climate model. They calculated 10 000-yr return surge levels and found no statistically significant change for the Dutch coast during the 21st century. Some climate modelling studies suggest there will be an increase in the frequency of westerly winds but there is no support for a change towards more Northerly (surge-favouring) winds. The contribution from high river discharge is not taken into account. Multiday precipitation extremes, however, are likely to increase in intensity (winter) (Kew et al., 2011). The combined probability of a storm surge and high discharge could therefore also change for a warmer climate. In addition, the number of barrier-closures is expected to increase (exponentially) with sea-level rise and the duration of closure will also increase (Van den Brink et al., 2005; Katsman et al., 2011), but we will not look into sea level rise here.

1.5 Idealised approach

There are multiple factors affecting both discharge and sea level, such as land use and tides. Rather than using discharge and surge models to encompass all complexities, we instead take a more idealised approach, using simple parameters as proxies for high

5   discharge and storm surge, calculated using a large global climate model ensemble which offers a good representation of natural variability. We study the effect of small changes to these parameters on the probability of a joint-event in order to gain some understanding of the sensitivity of the results to the choices made.

Our results will offer answers to two basic questions:

10   1. After extreme precipitation over the Rhine basin, what is the probability distribution of North Sea wind direction and strength compared with climatology? (Sects. 3.1–3.4.)

2. Is there an enhanced probability of a storm surge after a period of extreme precipitation over the Rhine basin? (Sects. 3.5–3.6.)

15   After comparing the current climate probabilities with those for future climate projections (Sect. 3.7), we will discuss these results in the light of the study by Van den Brink et al. (2005) (Sect. 4).

2 Methodology

2.1 Data set and study regions

20   All data used are derived from the ESSENCE data set (Sterl et al., 2008) a 17-member ensemble simulation spanning the years 1950–2100, generated from the ECHAM5/MPI-OM coupled global climate model. It has a horizontal resolution of T63 and 31 vertical hybrid atmospheric levels, and is forced by the SRES A1b scenario

(Nakićenović et al., 2000). The different ensemble members are formed by perturbing the initial state of the atmosphere, with ocean conditions unchanged.

We make use of the first 30-yr period, 1950–1980, to represent the current climate, and the final 30-yr period, 2070–2100, to represent the future climate. In both cases, we explore the winter season DJF alone. All wind variables are derived from daily averages of 10 m zonal and meridional wind components. Other variables extracted are daily precipitation, and mean sea level pressure.

Figure 1 illustrates the regions taken to be relevant for this investigation and the ESSENCE grid. The Rhine basin is represented by a box of 12-grid cells, centred over Germany. Precipitation is averaged over the box with equal weighting for each cell. Wind conditions are assessed within a box over the North Sea with equal weighting for each grid cell. The boundaries of the North Sea box were chosen based on the region of strong winds shown in the synoptic map for the strongest surge in ESSENCE found by Sterl et al. (2009) (their Fig. 2b). The default region is 2-cells wide and 4-cells long. The configuration is varied, as illustrated, as part of a sensitivity study.

We assume that the probability of a storm surge is enhanced when the wind is from the NNW direction. For this reason, we calculate the projection of the wind vector onto the NNW axis, as well as the resultant wind strength and direction over the North Sea box.

The NNW axis (unit vector) is denoted $\hat{s} = \cos\theta\hat{i} + \sin\theta\hat{j}$ where $\theta = -67.5°$ is the angle measured anticlockwise from the horizontal axis (convention in vector calculus) and $\hat{i}$ and $\hat{j}$ are unit vectors in the zonal and meridional directions.

The projection, w_1, of the wind vector, $\boldsymbol{v} = u\hat{i} + v\hat{j}$, onto the NNW axis, $\hat{s}$, is given by $w_1 = \boldsymbol{v} \cdot \hat{s} = u\cos(67.5°)\hat{i} - v\sin(67.5°)\hat{j}$.

The magnitude of the wind field is averaged over the North Sea box with equal weighting for each grid cell.

The wind direction representative for the North Sea box is given by the unit vector of the resultant wind vector over the N grid cells, i.e.

$$\hat{\boldsymbol{w}} = \frac{\sum_{k=1}^{N} \hat{\boldsymbol{v}}_k}{\left\| \sum_{k=1}^{N} \hat{\boldsymbol{v}}_k \right\|}, \tag{1}$$

where $\hat{\boldsymbol{v}}_k$ is the unit vector in the direction of the wind in a single grid cell k. The compass bearing, ϕ, (angle from which the wind is coming, measured clockwise from North following nautical convention) is given by the inverse tangent of the ratio of the zonal to meridional component of the resultant wind vector. This can be written as

$$\phi = \tan^{-1}\left(\frac{\sum_{k=1}^{N} u_k / \|\boldsymbol{v}_k\|}{\sum_{k=1}^{N} v_k / \|\boldsymbol{v}_k\|} \right) + 180°. \tag{2}$$

The default lag between the end of the n-day precipitation block and the timing of the wind assessment is set at 0, which is reasonable for multi-day precipitation sums. This is the lag for which correlation between 20-day precipitation sums and stream flow at Lobith is maximised (about 0.75). For 10-day precipitation sums, the correlation is maximised for a lag of 2 days, but is still quite high (about 0.72) for a lag of 0.

2.2 Definitions for extreme discharge and surge conditions

We make the following choices to identify extreme discharges and storm surges in the data set. We assume that a high discharge occurs if the quantile q_x^r (where x is fixed at 99 %) of n-day basin-averaged precipitation sums denoted by r_n (where n takes a value in the range of 1–20 days), is exceeded. The set of n-day precipitation sums meeting the condition $r_n > q_{0.99}^r$ is marked with an asterisk, r_n^*.

We assume that an imminent storm surge is expected when the North Sea daily average NNW wind component w_1 exceeds the distribution's quantile q_x^w. Here x is also chosen to be 99 %. The set of wind events meeting the condition $w_1 > q_{0.99}^w$ is marked with an asterisk, w_1^*.

If extreme discharge events and storm surges occur independently, we can expect the probability of observing a surge $P(w_1^*)$ to be fixed at $1 - x = 0.01$ regardless of (any extremes in) the precipitation history, i.e. $P(w_1^*|r_n^*) = P(w_1^*) = 0.01$.

Note that the 99 % quantile is a soft extreme, approximately one event per winter season, equivalent to a return period of 1 yr. We choose soft extremes in order to ensure that a reasonably sized sample of joint events is available in the data set (see next section for the expected sample size). Statistical methods can be used to estimate the return periods of extremes beyond those observed in the data, far into the tails of the individual event distributions. Modelling extremes of the *joint* events would be more challenging. However, we also wish to examine the synoptic (physical) evolution in the lead up to the extreme joint events, for which we require the events to be observed in the data series, as opposed to being modelled from it. In this study we therefore investigate soft extremes alone.

2.3 Assessing joint-probability and sampling error

For a 30-yr period, a 90-day DJF season and 17 ensemble members, ESSENCE provides $30 \times 90 \times 17 = 45\,900$ events. Note that we do not restrict the analysis to independent (non-overlapping) events. In total, 459 events will exceed the $q_{0.99}^r$ threshold by construction. If the probability of a storm surge is independent of precipitation history, we can expect on the order of 4–5 joint (high discharge and surge) events to occur by chance. If the events are not independent, we should see a significantly larger number of joint events, or a smaller number in the case of an inhibiting effect. We express the magnitude of change in the joint probability by a scale factor, S, obtained by normalising the result by the expected independent probability $P(w_1^*) \equiv 0.01$:

$$S_{\text{joint}} = \frac{P(w_1^*|r_n^*)}{P(w_1^*)}. \tag{3}$$

Naturally there will be some sampling error associated with the number of joint events that actually occur or the number that are expected to occur by chance. To obtain an

estimate of the amplitude of sampling error, we take 1000 random samples of the same size (459) as the precipitation-conditioned sample. From these samples, we obtain a range of PDFs for the wind direction, speed and NNW component. In this case, the exceedance of the climatological $q_{0.99}$ thresholds is given by

$$\widetilde{S}_{\text{joint}} = \frac{P(w_1^* | \widetilde{r}_n)}{P(w_1^*)}, \tag{4}$$

where the tilde denotes a quantity derived from a random sample.

We present figures for the distribution of exceedances Eq. (4) compared to the precipitation-conditioned sample Eq. (3). We also show the wind PDFs (not restricting to wind extremes) and their anomaly to the climatological PDFs for both the precipitation conditioned sample, $P(w_1 | r_{n*})$, and the random samples, $P(w_1 | \widetilde{r}_n)$.

2.4 Variable parameters

The number of joint events identified in the data set and, consequently, our estimate of the joint event probability could be sensitive to our choice of parameters defining the surge and discharge proxies. In this document we will look at the sensitivity of the results to the configuration of the North Sea wind assessment box and the precipitation interval, n.

It is also possible in our scheme to set a lag between the wind assessment and the peak of the weighted precipitation maximum (a centre of mass calculation) within a block. In the current study, we simply use the default set-up with zero lag.

There are several other variable parameters which may be varied in the set-up we have used. These will be mentioned in the final section.

3   Results

3.1   Climatology of current North Sea winds

In Fig. 2 the full season DJF wind climatologies (1950–1980) of wind direction (a), wind speed (b) and NNW wind components (c) are presented. Results for the future
[5] (2070–2100) are also included in this figure and subsequent figures but these will be commented on in Sect. 3.7. For the current climate, it is seen in Fig. 2a that the most common wind direction is SW, the least common is NNE, and the surge-favourable NNW direction (right-most bin) occurs with just over one third of the peak frequency. The peak frequency in Fig. 2c is for a slightly negative NNW wind component, which
[10] is consistent with Fig. 2a as the SW direction vector projects negatively onto the NNW axis. The $q_{0.99}^{w}$ threshold is $12.0\,\mathrm{m\,s^{-1}}$ in the positive NNW direction. We now examine how the wind distribution departs from the climatology, after a period of heavy precipitation.

3.2   Wind direction conditioned on preceding heavy precipitation

[15] Figure 3 shows the direction of North Sea wind on the day following an *n*-day period of heavy precipitation over the Rhine basin and the PDF's anomaly with respect to the full climatology of Fig. 2a. The 95 % range in frequency density obtained from the PDFs of 1000 random samples of the total population (described in Sect. 2.3) is presented as a shaded region to illustrate the magnitude of error due to sample size.
[20]   A significant departure from the climatological PDF (climatology effectively represented by the shaded band) is evident. For 1-day precipitation events (left hand column), the peak of the distribution is shifted clockwise with respect to climatology, favouring westerlies, whilst the NNW direction is not favoured more than in the climatology. For 2-day extremes (not shown) the peak rotates further towards the North.
[25] For 5-day precipitation extremes (middle column), the North-West quarter is favoured significantly and southerlies are suppressed. Following 20-day precipitation extremes

(right hand column), the NNW direction is still favoured more than for the climatology but the distribution of wind directions as a whole is relaxing back towards the climatological form.

3.3 Wind speed conditioned on preceding heavy precipitation

Following single-day precipitation extremes, there is also a shift of the wind speed distribution towards higher wind speeds (not shown). The mode, for example, increases from about $9 \, \mathrm{m \, s^{-1}}$ to $11 \, \mathrm{m \, s^{-1}}$. For larger n however, the wind speeds are not significantly different to the climatological distribution.

The $q_{0.99}$ exceedance is significant for $n = 1$ (Supplement, Fig. S1a). We can say that following a 1-day precipitation extreme, the wind speed is nearly 4 times more likely to be extreme than for climatology. For $n = 5$ (Fig. S1b) and $n = 20$ (Fig. S1c), there is an indication that higher exceedances than normal can be expected, but the departure from climatology is not significant.

3.4 NNW wind component conditioned on preceding heavy precipitation

We now look to see if there is any evidence of an enhanced probability of storm surge wind conditions after a period of extreme precipitation over the Rhine basin. Figure S2 in the Supplement shows the PDFs of the magnitude of the NNW wind component over the North Sea, following n-day precipitation extremes over the Rhine basin. A positive shift of the PDF is apparent for all n-day sums considered. The change is also significant for magnitudes exceeding $q_{0.99}^w$.

To illustrate the changes to the extreme end of the distribution, we display in Fig. 4 the $q_{0.99}^w$ exceedance of the precipitation-conditioned NNW wind components (triangle marker) as well as the distribution of $q_{0.99}^w$ exceedances obtained from 1000 random samples of the same size (histogram). The precipitation-conditioned exceedance is an estimate of the true joint probability, $P(w_1^* | r_n^*)$ but will be affected by the limited sample size. We expect the random sample exceedances to be distributed about the

climatological exceedance, which is 0.01 by construction, with a spread associated with the error due to sample size. When the precipitation-conditioned exceedance lies outside of the 99 % range of random sample exceedances (marked by dashed vertical lines), we assume that the probability of the joint event is significantly different to
5 climatology.

The exceedances of the $q_{0.99}^w$ threshold in Fig. 4 are seen to be significant for all n considered. For example, extreme NNW winds (black triangle) are 3–4 times more likely than the climatological $q_{0.99}^w$ exceedance when following 20-day extreme rainfall events over the Rhine basin (Fig. 4c).

10 **3.5 Sensitivity to the assessment location for wind conditions**

Figure 5a shows the impact on the estimated scaled joint probability, S_{joint} (Eq. 1), of changing the size and position of the North Sea box (see Fig. 1 for configurations) used to assess the NNW wind component. The joint probabilities are raised up to a factor of 5 above the unconditional probability of a surge, following a 2-day precipitation extreme.
15 For a 10-day precipitation extreme, S_{joint} ranges from about 2 to 4.3, depending on the region used for wind assessment. For a 20-day precipitation extreme, S_{joint} ranges between about 1.3 to 3.3. Box 1 and Box 2 give similar results for all n-day sums, and indicate larger joint probabilities at large n than the other boxes. Box 1 and 2 are more elongated than Box 3 and 4. The fact that we look for extreme winds in a
20 direction nearly parallel to the longest side of the box, may cause events featuring larger synoptic systems to be preferentially selected by the elongated boxes. Larger spatial and temporal correlations might then be expected, favouring larger joint probabilities of events over the Rhine Basin and the North Sea.

Van den Brink et al. (2004) use model wind data from a single location over the North
25 Sea to model surges. The location corresponds closest to the North-East most cell of Box 1, thus their wind input, and potentially their results, should be most similar to the more weakly anomalous results attained from Box 3 or 4.

That the largest joint probabilities attained for all boxes are found following 2-day precipitation events probably signifies that the same synoptic system is responsible for heavy rain and the subsequent surge created by the increase in Northerly winds as the system passes (Fig. 5a). A second peak in joint probability occurs at 10 days for Box 1, 2 and 3. The precipitation is likely to have been generated from more than one synoptic system – the first of which does not necessarily contribute to the surge conditions, as 10 days is an adequate length of time for the full passage of at least 2 depressions. In the next section, the evolution of the systems involved is clarified further.

3.6 SLP composites

In Fig. 6 we present the full SLP climatology for the DJF season for ESSENCE (Fig. 6a) alongside similar results from ERA-Interim for reference (Fig. 6b). Both show a region of low pressure extending across the Atlantic between Greenland and the UK – the storm track.

SLP composites and their anomalies of days satisfying the wind and precipitation criteria are shown in Fig. 7. The composite of days satisfying the NNW extreme wind condition (a) shows a low pressure centre over Southern Scandinavia and a ridge North of the Azores and another low between Greenland and Newfoundland. Depicted as an anomaly with respect to the total climatology (b), the composite reveals an East-West SLP dipole centred over the North Sea. The location of the SLP minimum is in good agreement with the surge-favourable conditions reported in the literature.

Figure 7c–d shows the SLP composite and anomaly for days satisfying the precipitation criterion for 20-day precipitation sums. Similar figures for 1-day and 10-day sums are found in the Supplement, Fig. S3a–d. For the 1-day event, the dominant feature is a negative SLP anomaly centred over Denmark. For the multi-day sums, a weaker negative SLP anomaly is featured but is positioned further to the south east, as well as a positive anomaly to the west of France. Note that the reference date used for these composites is the last date in the n-day period, meaning that the rainfall has fallen over the n-days preceding the synoptic situation shown. For all three precipitation

Title Page

Abstract | Introduction

Conclusions | References

Tables | Figures

◄ | ►

◄ | ►

Back | Close

Full Screen / Esc

Printer-friendly Version

Interactive Discussion

summation periods shown, the SLP anomaly configuration favours Northerly or North-westerly wind flow over the North Sea.

Figure 7e–f displays the SLP composite and anomaly satisfying both the surge and 20-day precipitation criteria. Similar figures for the joint condition for 1-day and 10-day precipitation sums are found in the Supplement, Fig. S4. The anomaly dipole structures are heavily influenced by the requirement to fulfill the NNW wind criterion. The dipole pattern is similar to that for the composite of days satisfying the wind conditions alone (Fig. 7b) but the amplitude is stronger. There is much more ridging evident over the Atlantic, compared to the composites conditioned on precipitation only (Fig. 7c).

Figure 8 shows the composite for the joint event for $n = 20$ as a temporal sequence from 1 day before the reference date to 20 days before the reference date. Over this period, two synoptic regions of low pressure pass central Europe in the composite (see labels A and B in Fig. 8). In the Supplement, a single event contributing to this composite is singled out for comparison (Fig. S5). There are approximately 6 synoptic low pressure systems (labels A to F) and their troughs that contribute to precipitation over the Rhine basin. Clearly a succession of low pressure systems contribute to the precipitation maximum. A notable feature is the strong ridging over the east Atlantic that causes low F to move south over Europe and brings Northerly winds over the UK and the North Sea. This feature – the rotation of a synoptic region of low pressure about a strong ridge, is also present in the composite (Fig. 8).

3.7   Joint events in a future climate

The same analysis has been carried out for the future years 2070–2100, using Box 1 to assess the North Sea wind conditions.

The DJF climatology (Fig. 2, grey dots) shows some small changes compared to the current period. The PDF of bearings becomes more peaked, still with a maximum from the SW direction. The frequency of winds from the NW quarter is very slightly reduced. There is a small widening of the PDF in wind speed, giving a slightly higher 99 % quantile. The 99 % quantile of the PDF for the NNW wind component is lowered

by a small amount (from 12.0 to 11.8 m s^{-1}). This suggests there will not be a great deal of change in surge conditions, and if anything, the probability of extreme surges would be reduced.

Following 1-day precipitation extremes, the frequency of wind from the W to NW directions, is less pronounced in the future (Fig. 3a and d, grey dots). However the frequency of winds from the NNW direction remains about the same. Following 5-day precipitation extremes, the current and future wind distributions are very similar (Fig. 3b and e, compare grey dots to histogram) despite the PDF of the total wind climatology becoming more peaked (Fig. 3b, grey lines). Following 20-day precipitation extremes, the future wind distribution is closer to the full climatology than for the current climate (Fig. 3c and f).

Regarding the NNW wind component after a precipitation extreme, a shift away from climatology towards more positive values is still evident in the future PDF (Supplement, Fig. S2, grey dots). The departure from climatology is generally less than for the current climate for $n = 1$ and $n = 20$. For $n = 5$, the current and future wind samples are very similar. For $n = 20$ the joint event probability is, by contrast to the current climate, not significant (see exceedance of $q_{0.99}^{w}$ in Fig. 4c) and in the particular sample our dataset produces, is less (but not significantly less) than the climatological probability. If we use the current climate quantile definition of a $n = 20$ precipitation extreme, the joint event probability is still insignificant ($S_{\text{joint}} \sim 0.014$, not shown). Following a shorter precipitation extreme of $n = 5$, the chance of a surge is similar to the current climate, i.e. raised about 4 times above the independent probability.

4 Summary and discussion

After extreme rain over the Rhine basin, we find that the probability distribution of North Sea wind strength and direction shows significant departures from the 1950–1980 climatology. Wind directions in the West to North West quarter are favoured following

both single and multi-day precipitation events, whilst the climatological mode direction, SW, is less favoured.

Sampled over all directions, wind speeds are significantly larger than climatology only when following extreme precipitation events of short duration. The magnitude of the wind projected in the NNW direction, however, increases over climatological values also for multiday events, including extremes ($w_1 > q^w_{0.99}$). The exceedance of the $q^w_{0.99}$ threshold was shown to be outside of the range that can be expected from sampling error. These changes therefore suggest that the probability of a surge conditioned on preceding heavy precipitation is indeed larger than when independence is assumed.

The probability of a NNW wind extreme conditioned on a preceding 20-day rain extreme (as seen in Fig. 5) is over 3 times greater than for the unconditioned case (using Box 1 of Fig. 1 for the wind conditions). Although this increase is significant, it is still quite small – approximately 97 % of surge conditions occur without a preceding 20-day precipitation extreme. Figure 9 illustrates the results schematically with Venn diagrams. The area of overlap between the set w^*_1 of wind extremes and the set r^*_{20} of precipitation extremes increases more than 3-fold between panel a and b, but the joint events are still a tiny fraction of the two individual sets.

To place these results in context with those of Van den Brink et al. (2005), we produced our own version (Fig. 10) of their Fig. 6b. We plot 20-day precipitation sums instead of Rhine discharge, and North Sea NNW wind component instead of the Sea Level at Hoek van Holland and, for clarity, display density contours rather than a scatter plot. Just as for Fig. 6b of Van den Brink et al. (2005), there is no correlation to be seen between the two variables (black contours, Fig. 10).

In addition, we simulated a distribution for which we know that the wind and precipitation variables are independent (grey contours). It is made by replacing the actual wind values, following each 20-day precipitation sum, with wind values selected randomly from all days. A comparison between the two distributions (black and grey) allows the way in which the actual distribution departs from the assumptions of independence to be visualised. Shaded black (grey) regions indicate where the actual distribution's

density is larger (smaller) than that of the independent probability distribution for a given NNW wind component. Although we have only investigated soft extremes, it is evident that the departures from the independent distribution are greatest in the top right hand segment of the figure, i.e. in the tail of the joint distribution. The shift of the PDF for the conditioned samples with respect to the climatology (Supplement, Fig. S2c) can also be gleaned from this figure, by noting the pattern of grey and black areas in the regions exceeding the $q_{0.99}$ thresholds (dashed lines).

Inspection of the SLP composites satisfying the joint conditions for wind and rain extremes shows an intuitive sequence where, for a 20-day extreme precipitation sum, rain is accumulated from at least 2 synoptic systems and the North Sea surge conditions are generated at the rear of the final system as it passes across southern Scandinavia.

Projections for the future (2070–2100) suggest that surges following multiple day precipitation extremes will be less likely than at present. The assumption of independence between extreme surge and discharge events was found to valid for the longer multiple day precipitation sums ($n = 20$) in the ESSENCE data set. It is known that DJF westerly wind components increase in the ESSENCE data set (ECHAM5/MPI-OM) with climate change (Van Ulden and van Oldenborgh, 2006) but that there is insignificant change to the Northerly wind component and the likelihood of storm surges (Sterl et al., 2009). The increased frequency of westerlies appears to negatively impact the probability of an extreme *joint* surge-discharge event, when the discharge extreme results from multiple days of precipitation. In multiple-day extremes, the precipitation generally results from the passage of several systems, and the discharge and surge events may be decoupled (not from the same system). The chance that the days subsequent to a precipitation extreme will bring westerlies rather than surge-favourable winds is enhanced in the future climate.

The joint probability was found to be sensitive to the North Sea box dimensions used for the wind conditions and to the length of the precipitation sum used as a proxy for discharge. It would be instructive and straight forward to test the following parameters in an extended sensitivity analysis: Rhine basin assessment region dimensions, lag between

the precipitation reference date and the wind assessment, position of reference date in precipitation block, start date and number of years included in the climatology, season, axis of projection for winds, duration of wind condition, quantiles defining the extreme events.

5   Whilst this simple set up is useful for preliminary investigations, there are several important factors which introduce further uncertainty and should be taken into account in a more thorough investigation using sophisticated surge and discharge models. These are, for example, the contribution to discharge of rapid snow melt, the possibility of dam breeches upstream, the river basin configuration and tides. Changes to the joint

10   probability of extreme surge and discharge events in the future are likely from sea-level rise, increases in storm frequency or intensity, and earlier and potentially more rapid snow melt.

We particularly recommend a comparison of the present results for the current climate with the output of coupled surge-discharge models when driven by the same

15   global ensemble (containing the same synoptic systems).

A major question remaining is how these results extend to more extreme events with multiple-year return periods.

Supplementary material related to this article is available online at: http://www.nat-hazards-earth-syst-sci-discuss.net/1/111/2013/

20   **nhessd-1-111-2013-supplement.pdf.**

References

Katsman, C. A., Sterl, A., Beersma, J. J., van den Brink, H. W., Church, J. A., Hazeleger, W., Kopp, R. E., Kroon, D., Kwadijk, J., Lammersen, R., Lowe, J., Oppenheimer, M., Plag, H. P., Ridley, J., von Storch, H., Vaughan, D. G., Vellinga, P., Vermeersen, L. L. A., van de Wal, R. S. W., and Weisse, R.: Exploring high-end scenarios for local sea level rise to develop flood protection strategies for a low-lying delta – the Netherlands as an example, Climatic Change, 109, 617–645, doi:10.1007/s10584-011-0037-5, 2011. 115

Kew, S. F., Selten, F. M., Lenderink, G., and Hazeleger, W.: Robust assessment of future changes in extreme precipitation over the Rhine basin using a GCM, Hydrol. Earth Syst. Sci., 15, 1157–1166, doi:10.5194/hess-15-1157-2011, 2011. 115

Nakićenović, N., Alcamo, J., Davis, G., de Vries, B., Fenhann, J., Gaffin, S., Gregory, K., Grubler, A., Jung, T. Y., Kram, T., La Rovere, E. L., Michaelis, L., Mori, S., Morita, T., Pepper, W., Pitcher, H. M., Price, L., Riahi, K., Roehrl, A., Rogner, H.-H., Sankovski, A., Schlesinger, M., Shukla, P., Smith, S. J., Swart, R., van Rooijen, S., Victor, N., and Dadi, Z.: Special Report on Emissions Scenarios: A Special Report of Working Group III of the Intergovernmental Panel on Climate Change, 599 pp., Cambridge Univ. Press, Cambridge, UK, 2000. 117

Sterl, A., Severijns, C., Dijkstra, H., Hazeleger, W., van Oldenborgh, G. J., van den Broeke, M., Burgers, G., van den Hurk, B., van Leeuwen, P. J., and van Velthoven, P.: When can we expect extremely high surface temperatures? Geophys. Res. Lett., 35, L14703, doi:10.1029/2008GL034071, 2008. 116

Sterl, A., van den Brink, H., de Vries, H., Haarsma, R., and van Meijgaard, E.: An ensemble study of extreme storm surge related water levels in the North Sea in a changing climate, Ocean Sci., 5, 369–378, doi:10.5194/os-5-369-2009, 2009. 113, 115, 117, 128

Van den Brink, H. W., Können, G. P., Opsteegh, J. D., van Oldenborgh, G. J., and Burgers, G.: Improving 10^4-year surge level estimates using data of the ECMWF seasonal prediction system, Geophys. Res. Lett., 31, L17210, doi:10.1029/2004GL020610, 2004. 113, 114, 123

Van den Brink, H. W., Können, G. P., Opsteegh, J. D., van Oldenborgh, G. J., and Burgers, G.: Estimating return periods of extreme events from ECMWF seasonal forecast ensembles, Int. J. Climatol., 25, 1345–1354, 2005. 112, 114, 115, 116, 127

Van der Made, J. W.: Design levels in the transition zone between the tidal reach and the river regime reach, Hydrology of Deltas, Vol. 2 of Proceedings of the Bucharest Symposium, May 1969, 257–246, 1969. 114

Simultaneous occurrence of surge and discharge extremes

S. F. Kew et al.

Title Page

Abstract	Introduction
Conclusions	References
Tables	Figures

◀◀   ▶▶

◀   ▶

Back   Close

Full Screen / Esc

Printer-friendly Version

Interactive Discussion

van Ulden, A. P. and van Oldenborgh, G. J.: Large-scale atmospheric circulation biases and changes in global climate model simulations and their importance for climate change in Central Europe, Atmos. Chem. Phys., 6, 863–881, doi:10.5194/acp-6-863-2006, 2006. 128
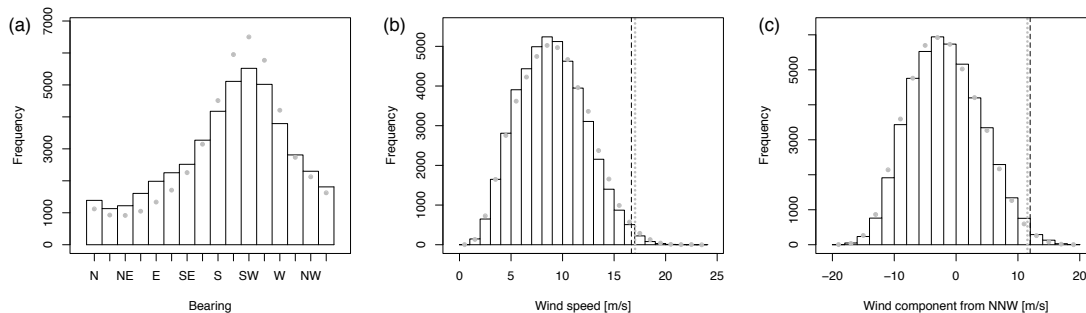
Simultaneous occurrence of surge and discharge extremes

S. F. Kew et al.
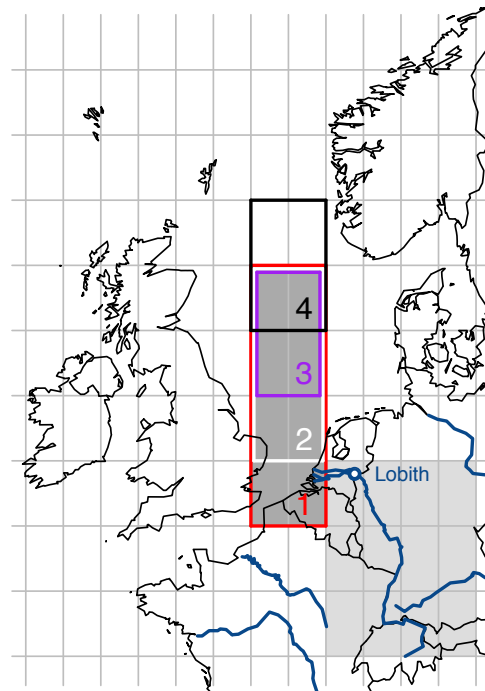
Fig. 1. ESSENCE grid cells selected to represent the Rhine basin (light grey shading) and assess the North Sea wind conditions favourable for surges (dark grey shading). Numbered boxes indicate the configurations used for sensitivity testing in Sect. 3.5.

Fig. 2. DJF Climatologies of wind directions **(a)**, wind speed **(b)** and NNW wind component **(c)** averaged over the North Sea box (shaded dark grey in Fig. 1). Bars show the distribution for the current climate (1950–1980) and dots for the future (2070–2100). The dashed vertical lines in **(b)** and **(c)** mark the location of the 99 % quantiles of the current (black) and future (grey) climatologies.

Full Screen / Esc

Printer-friendly Version

Interactive Discussion
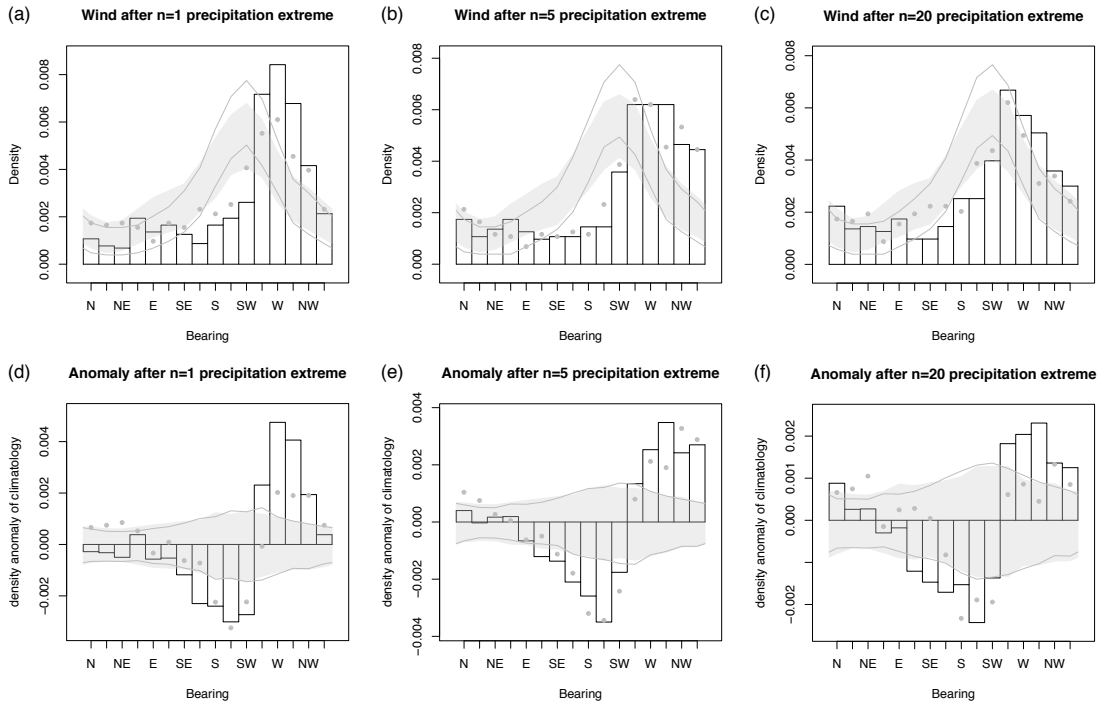
Fig. 3. Wind directions following extreme (bars for current climate, dots for future) and random samples (95 % density range, shaded for current climate, outlined for future) of *n*-day precipitation sums (left) and their anomaly (right) with reference to the climatology (1950–1980 for current climate, 2070–2100 for future).
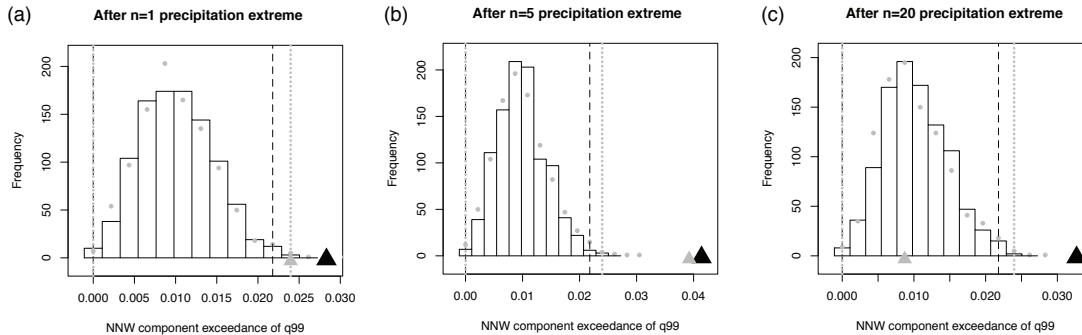
Fig. 4. Exceedance of the 1950–1980 climatological $q_{0.99}^{w}$ for the NNW wind component following extreme n-day precipitation sums (black triangle for current climate, grey for future) and 1000 random samples of the same size (black bars for current climate, dots for future). The vertical lines enclose 99 % of the 1000 samples (black dashed for current climate, grey dotted for future).
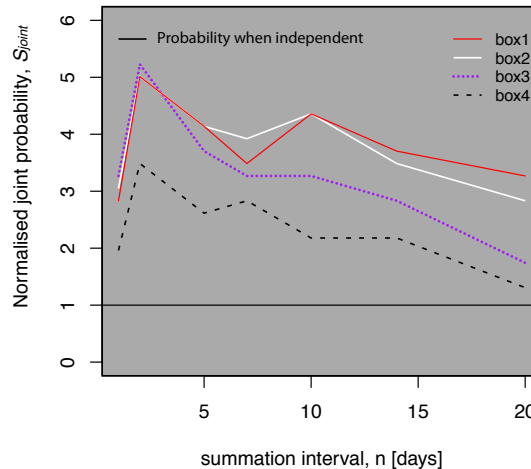
Fig. 5. Summary of effect of changing North Sea box dimensions on the normalised joint probability S_{joint} (exceedances of the climatological $q_{0.99}^{w}$) for NNW wind component (1950–1980). Configurations of the four North Sea boxes can be seen in Fig. 1 with the same colour coding.
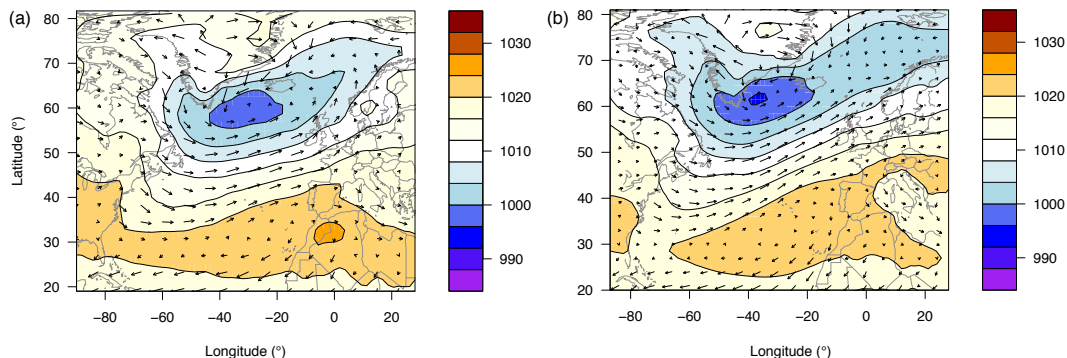
Fig. 6. (a) ESSENCE SLP climatology in hPa (45 900 entries) for DJF 1950–1980, **(b)** ERA-Interim SLP climatology (1.5° × 1.5°) for DJF over the 30-yr period 1979–2009.
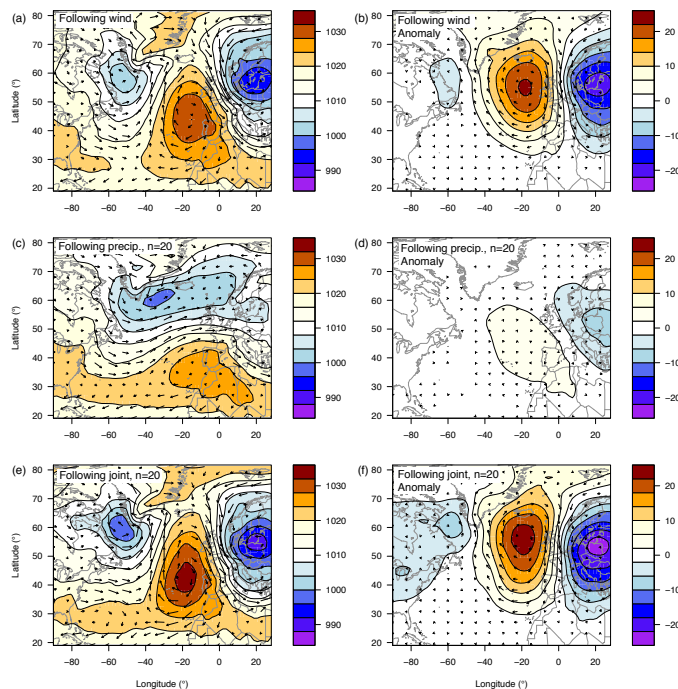
Fig. 7. (a) Composite satisfying North Sea wind criteria (459 entries) and its anomaly **(b)** with respect to full climatology (Fig. 6a). **(c)** Composite satisfying 20-day precipitation criteria (459 entries), for which the precipitation has fallen over the 20-days preceding the synoptic situation shown, and its anomaly **(d)** with respect to the full climatology in Fig. 6a. **(e)** Composite jointly satisfying the wind and 20-day sum precipitation criteria (15 events) and its anomaly **(f)** with respect to the full climatology in Fig. 6a.
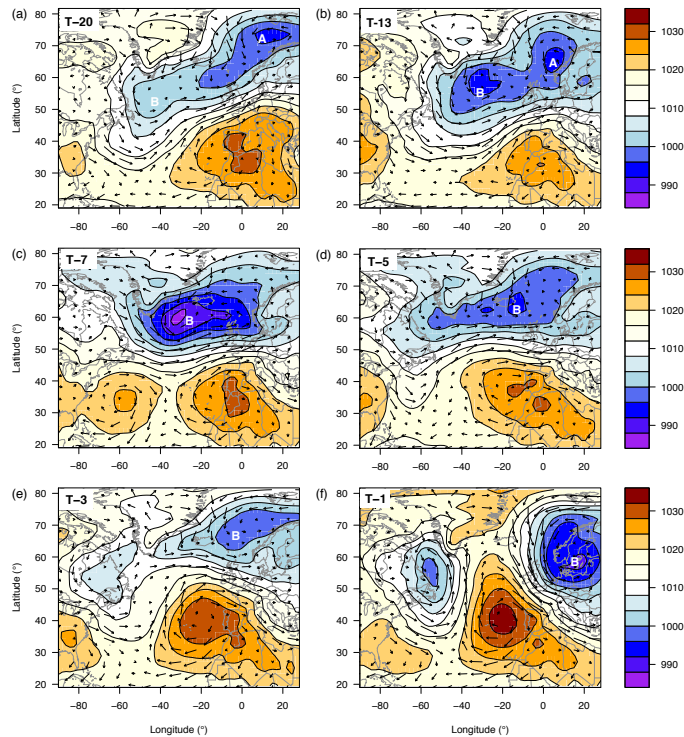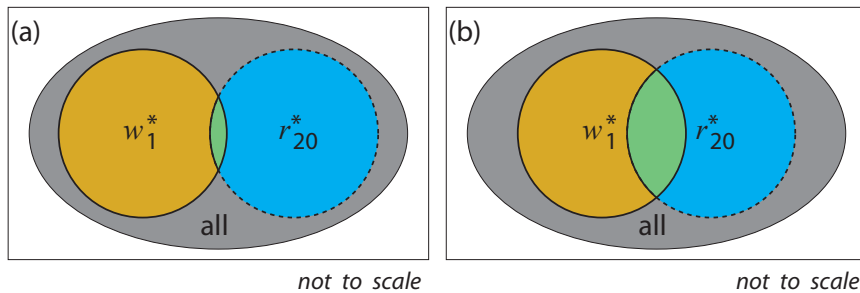
Fig. 8. Evolution of the SLP composite satisfying the joint extreme conditions ($n = 20$ for precipitation) at times T (15 events). Time references are in days relative to T.

Fig. 9. Venn diagrams showing schematically the set of wind extremes (w_1^*, yellow) and 20-day precipitation extremes (r_{20}^*, blue) as subsets of the total data available (grey) and their overlap (green). By construction, both the w_{1*} and r_{20}^* subsets are 1% of all days. If the wind extremes are independent of the precipitation extremes, the probability of the joint event (green overlap) is $P(w_{1*})P(r_{20}^*) = 0.01\%$ of the total number of days, or equivalently, 1% of wind extremes occur by chance within the subset of precipitation extremes **(a)**. However, ESSENCE data shows the percentage of joint events (green overlap) to be 2–4 times larger **(b)**, considering 20-day precipitation events. There are still however a large proportion of wind extremes (**b**, yellow) that do not overlap with the set of extreme precipitation events.
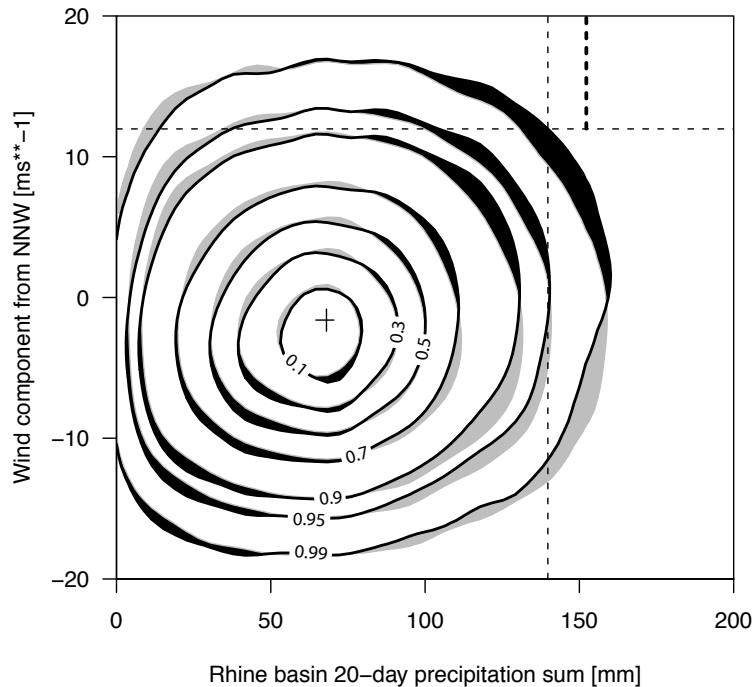
Fig. 10. Data density (kernel density estimation) for Rhine basin 20-day precipitation sums (DJF, 1950–1980) against the North Sea NNW wind component evaluated on the last of the 20-days. Labels indicate the proportion of the data cloud enclosed by the contours. Black contours are for the pure results from the ESSENCE data set. Grey contours show how the distribution would look if the two variables were independent. Black (grey) shading is used where the true distribution's frequency density exceeds (undercuts) that of the independent distribution for the same NNW wind speed. Thin dashed lines show the 99 % quantiles for each variable estimated from the pure data. The thick dashed line shows the 99% precipitation quantile of the sub group w_1^* satisfying $w_1 > q_{0.99}^w$. The cross marks the mean of the 2-D distribution.